◆ Human Brain Mapping 33:2920–2931 (2012) ◆

Tagging Cortical Networks in Emotion: A Topographical Analysis

Andreas Keil,[1]* Vincent Costa,[1] J. Carson Smith,[2] Dean Sabatinelli,[3] E. Menton McGinnis,[1] Margaret M. Bradley,[1] and Peter J. Lang[1]

[1]*Center for the Study of Emotion and Attention, University of Florida, Gainesville, Florida*
[2]*Department of Kinesiology, University of Maryland, College Park, Maryland*
[3]*Department of Psychology, University of Georgia, Athens, Georgia*

Abstract: Viewing emotional pictures is associated with heightened perception and attention, indexed by a relative increase in visual cortical activity. Visual cortical modulation by emotion is hypothesized to reflect re-entrant connectivity originating in higher-order cortical and/or limbic structures. The present study used dense-array electroencephalography and individual brain anatomy to investigate functional coupling between the visual cortex and other cortical areas during affective picture viewing. Participants viewed pleasant, neutral, and unpleasant pictures that flickered at a rate of 10 Hz to evoke steady-state visual evoked potentials (ssVEPs) in the EEG. The spectral power of ssVEPs was quantified using Fourier transform, and cortical sources were estimated using beamformer spatial filters based on individual structural magnetic resonance images. In addition to lower-tier visual cortex, a network of occipito-temporal and parietal (bilateral precuneus, inferior parietal lobules) structures showed enhanced ssVEP power when participants viewed emotional (either pleasant or unpleasant), compared to neutral pictures. Functional coupling during emotional processing was enhanced between the bilateral occipital poles and a network of temporal (left middle/inferior temporal gyrus), parietal (bilateral parietal lobules), and frontal (left middle/inferior frontal gyrus) structures. These results converge with findings from hemodynamic analyses of emotional picture viewing and suggest that viewing emotionally engaging stimuli is associated with the formation of functional links between visual cortex and the cortical regions underlying attention modulation and preparation for action. *Hum Brain Mapp 33:2920–2931, 2012.*

Key words: dense-array EEG; emotion; motivation; arousal; picture perception

INTRODUCTION

Heightened perceptual sensitivity when processing cues related to threat or reward is adaptive for both humans and animals. Studies using hemodynamic imaging in humans have provided evidence for activity in large-scale functional circuits during appetitive and aversive processing, whose activity is related to other measures of emotional engagement [Costa et al., 2010; Lang and Bradley, 2009]. For instance, research using functional magnetic resonance imaging (fMRI) has established that viewing pictures with emotionally arousing content (pleasant or unpleasant) is associated with greater activation in extrastriate areas of the occipital cortex, compared to viewing neutral pictures [Lang et al., 1998]. Signal increases during emotional processing are also evident in occipital and parietal cortex [Bradley et al., 2003] and the amygdala [Sabatinelli et al., 2005], as well as in the inferotemporal cortex and anterior cingulate cortex [Sabatinelli et al., 2007;

*Correspondence to: Andreas Keil, Center for the Study of Emotion and Attention, University of Florida, Gainesville, Florida, USA. E-mail: akeil@ufl.edu

Received for publication 3 March 2011; Revised 30 May 2011; Accepted 24 June 2011

DOI: 10.1002/hbm.21413

Published online 23 September 2011 in Wiley Online Library (wileyonlinelibrary.com).

Vuilleumier and Driver, 2007]. Using ultrarapid fMRI scanning, activation of the bilateral amygdala, and inferotemporal cortex in emotional processing were found to occur earlier than extrastriate visual cortex activation [Sabatinelli et al., 2009]. This finding supports a hypothesis of re-entrant facilitation of perceptual analysis during emotional engagement that is consistent with both animal [Desimone, 1996] and human [McMains et al., 2007] studies of selective attention. Computational models of re-entry exist, which predict changes in lower-tier visual cortex sensitivity to locations and features by feedback projections originating in more anterior structures such as the frontal and parietal cortex [Hamker, 2005; Yantis, 2008].

Here, we examine functional coupling between visual and higher-order extra-visual cortices during emotional processing. Non-invasive methods of measurement, such as human electroencephalography (EEG) or magnetoencephalography (MEG) are well suited to examine functional links between cortical regions as they provide a better time resolution than hemodynamic methods, at the cost of spatial specificity. In particular, the use of steady-state visual evoked potentials (ssVEPs), a continuous brain response elicited by flickering visual stimuli, allows the assessment of large-scale neural interactions between visual cortex and other cortical structures. Steady-state VEPs are recorded on the scalp as an oscillatory waveform that has the same fundamental frequency as the flickering stimulus [Regan, 1989]. Because the ssVEP is narrowly defined in the frequency domain (i.e., as the portion of the brain's electrical response at the driving frequency), it can be extracted as a clean and reliable signal from noisy neurophysiological time series, or from single trials [Keil et al., 2008].

Although the ssVEP primarily reflects sensory responses, it may be sensitive to higher-order processes as well, depending on the duration of the stimulus cycle [Herrmann, 2001]; with slower stimulation (<15 Hz), the scalp-recorded ssVEP probably includes electrocortical signals originating in secondary and higher-order cortical areas to which the activity spreads until the next excitation occurs [Di Russo et al., 2006]. Thus, topographical analyses of ssVEPs highlight cortical regions that are engaged reliably during each cycle of the flickering stimulus train. Importantly, regions that are coupled with visual cortical areas at a different temporal rate, or not engaged repetitively with each cycle of the stimulus, will not be indexed in this analysis.

Previous studies have found that the amplitudes of ssVEPs are sensitive to affective and attentional features of experimental tasks, including spatial selective attention [Müller et al., 2003], executive control [Silberstein et al., 1995], learned motivational relevance [Moratti and Keil, 2005, 2009], and emotional stimulus content [Keil et al., 2003; Kemp et al., 2002]. Granger causality analyses of ssVEP signals during picture viewing provided evidence for re-entrant modulation of early visual processing as a function of the pictures' emotional content [Keil et al., 2009]. Extending this previous work, the present study used the information contained in individual neuroanatomy and dense-array ssVEP recordings to identify rapidly and coherently engaged cortical networks during emotional processing.

The topographical distribution of the amplitude and phase response to a flickering stimulus at a defined frequency can be used to tag brain locations that are involved in processing that stimulus at the specified frequency. Measures of coherence or phase-locking (temporal stability) of the signal over time can be quantified by examining how stimulus-locked averaging across multiple epochs or within a viewing period affects the phase and amplitude of the signal [Lachaux et al., 2003]. Scalp regions with high amplitudes at the tagging frequency are interpreted as being coactive and can be further examined using coefficients of inter-site coherency at the stimulus frequency. This method of identifying coherently active cortical networks depends on a valid spatial representation of the signal, which minimizes spurious inter-site coherence, e.g., due to dipolar projection of the same underlying source, or to volume conduction effects [Michel et al., 2004].

In the present study, individual structural MR images were used to construct realistic volume conductor models for beamformer source projection [Ward et al., 1999] of the ssVEP evoked by affective pictures flickering at 10 Hz. Beamformers can be regarded as spatial bandpass filters that select activity relative to a location in the brain volume. By scanning multiple, densely localized sites in the brain volume, tomography-like source projections can be obtained. Because the spatial filters rely on the temporal or spectral covariance (coherence) of spatially separate brain regions, beamformer-based methods suppress effects of sources that are highly correlated in time, which helps to reduce effects of volume conduction on the estimated source configuration. As a consequence, beamformers can be effectively used for spatio-temporal analysis of activity in coherently active neural networks in EEG, where false positive coherencies are a concern [Gross et al., 2001]. For the present purpose, this approach is particularly advantageous because (1) it relies on individual head geometry and sources can be constrained to the cortical gray matter, which is the tissue of interest in this study, (2) it does not require fitting of a dipole model with limited sources, the number, orientation, or location of which needs to be known a-priori, and (3) in our implementation, it uses spectral density estimates for the dominant current direction at a given source location [see Gross et al., 2001] and thus does not introduce a systematic bias on the phase information.

Previous work has used parameters of scalp-recorded oscillatory brain activity to describe the spatio-temporal properties of cortical networks involved in affective perception [Aftanas et al., 2004]. For instance, phase synchrony has been measured between sites in a linearly estimated (minimum-norm) source space when viewing emotional pictures [Keil et al., 2007]. Regression-based

studies of oscillatory activity with MEG have pointed to modulation of widespread dorsal and ventral cortical areas of visual cortex, linearly varying with peripheral and behavioral measures of emotional reactivity [Moratti and Keil, 2005, 2009]. Network analyses based on Granger causality have provided directional descriptions of cortico-cortical connections, suggesting re-entrant ventral and dorsal projections into medio-occipital visual cortex when viewing emotionally arousing stimuli [Keil et al., 2009]. Although providing support for the hypothesis that cortico-cortical re-entry has a role in modulating visual cortex in emotional perception, previous studies could not systematically address questions related to the location of the efferent areas of re-entry, or whether re-entry is present in each cycle of the ssVEP. If reliable amplitude and coherence modulations of the ssVEP were observed outside lower tier visual areas, this would imply that a functional network of visual and potentially extravisual structures oscillates at the same rate, entrained by the visual flicker.

These questions were examined here by comparing the ssVEP topography when viewing pleasant, neutral, and unpleasant pictures in a beamformer source estimation based on individual head and brain geometry. Amplitude and inter-site coherence measures were used to describe the location and timing of the functional cortico-cortical networks that co-engage in time with every on/off cycle of a stimulus in a repetitive stream. On the basis of previous research, we expected to find greater amplitude in extended visual cortex for emotionally arousing compared to neutral pictures. We also expected that higher-order areas, particularly in the parietal, anterior temporal, and frontal cortex, which underlie the rapid allocation of visual resources to emotional cues on a trial-by-trial basis, would be tagged using this method, and would be more strongly engaged when viewing emotionally arousing, compared to neutral pictures.

METHODS

Participants

Eleven right-handed students (five male) with normal or corrected-to-normal vision ranging in age from 18 to 21 years (mean age 18 years, 10 month) gave informed consent to participate in the study and were given class credit for participation.

Stimuli and Design

Sixty color pictures were selected from the International Affective Picture System [Lang et al., 2008] to form six content categories. Pleasant pictures consisted of 10 erotic couples and 10 cute animals; neutral pictures consisted of 10 persons and 10 scenes with daily activities; unpleasant pictures consisted of 10 mutilated bodies and 10 animal threat scenes. The IAPS picture numbers are given in the Appendix. Normative ratings of hedonic valence for pictures in these categories differed (pleasant: 7.37, neutral: 5.08, unpleasant: 2.69), as did normative ratings of emotional arousal (pleasant: 5.38, neutral: 3.40, unpleasant: 6.24). The pictures were projected on a screen using a digital projector, connected to the graphics card of a control computer and set to a vertical frame rate of 60 Hz. Pictures subtended a visual angle of 10° horizontally and of 7° vertically. A fixation point was marked in the center of the screen and was present throughout the experiment. Each picture was presented for 6,000-ms flickering at a rate of 10 Hz (thus containing 60 on/off cycles), with the picture shown for 33.33 ms, followed by 66.67-ms black screen during each cycle. Each inter-trial interval lasted at least 12 s.

Electrophysiological Recordings

EEG was recorded continuously from 257 electrodes using an Electrical Geodesics^{TM} system digitized at a rate of 250 Hz, using Cz as a recording reference. Impedances were kept below 50 kΩ, as recommended for the Electrical Geodesics high input-impedance amplifiers. A subset of EGI net electrodes located at the outer canthi as well as above and below the right eye was used to determine the horizontal and vertical electrooculogram. All channels were preprocessed on-line by means of 0.1 Hz high-pass and 100 Hz low-pass filtering.

Structural MRI

T1-weighted anatomical volumes were acquired for each participant in a separate session using a Siemens 3T Allegra MR scanner. The prescription specified 160 sagittal slices, with 1-mm isotropic voxels in a 256-mm field of view. Offline, the anatomical volumes were manually transformed to Talairach-Tournoux coordinates by identifying fiducial markers that aligned the anterior–posterior axis to the anterior and posterior commissures and the inferior-superior axis to the mid-sagittal fissure. The aligned anatomical volume was then registered to the Montreal Neurological Institute (MNI) brain atlas. This procedure yields alignments comparable to those obtained using automated methods based on multi-parameter affine transformation.

Procedure

Participants were greeted and informed about the experimental procedures. They participated in two sessions, one MRI session, in which structural volumes were collected as described above, and one EEG session. The two sessions were scheduled in a counter-balanced order across participants. In the EEG session, the sensor net was applied and participants viewed two blocks of pictures, each consisting of the same 60 pictures. During the first block, the EEG was recorded; during the second block, affective ratings of valence and arousal were obtained using the Self Assessment Manikin [SAM, Lang, 1980].

The order of the stimuli within each block was pseudo-randomized with the restriction that no more than three pictures in the same affective category could occur in a row. A central fixation point was present throughout the study to aid participants in maintaining their gaze in the center of each picture. They were instructed to avoid eye movements and eye blinks and to view the pictures while they were on the screen.

Data Reduction and Artifact Control

Continuous data were low-pass filtered at a frequency of 40 Hz (48 dB/octave) and reduced using a procedure developed by [Junghöfer et al., 2000] for segmentation and artifact correction. Epochs of 12,000 ms (6,000 ms pre-, 6,000 ms post-onset of the flickering pictures) were obtained from the continuously recorded EEG, which ensured comparable signal-to-noise and identical frequency resolution for the frequency-domain estimates in the pre- (i.e., baseline) and poststimulus segments. The artifact rejection procedure used distributions of amplitudes, standard deviations, and change values to identify channels and trials that contain artifacts. Recording artifacts were first detected using the recording reference (i.e., Cz), and global artifacts subsequently detected using the average reference. In a next interactive step, distinct sensors from particular trials were removed based on the distribution. Data at eliminated electrodes were replaced with a statistically weighted spherical spline interpolation from the full channel set [Junghöfer et al., 1997]. Spline interpolation may make channels less independent and thus reduce the rank of the data matrix subjected to the beamformer estimate. As a consequence, we ensured that the three conditions (pleasant, neutral, unpleasant pictures) were comparable with respect to the amount and location of channels interpolated. The maximum number of approximated sensors in any trial, across conditions and participants, was 28. The SCADS procedure requires that interpolated channels are not in the same location in trials entering an average. Thus, topographies with rejected sensors were checked against a test topography to avoid interpolation artifacts, e.g., due to a region with consistently bad sensors. Spherical spline interpolation was used both for approximation of sensors and illustration of voltage maps [Junghöfer et al., 1997]. Single trials with excessive eye-movements and blinks, or with more than 28 channels containing artifacts were discarded. Trials that showed remaining ocular artifacts, based on visual inspection of the vertical and horizontal EOG computed from a subset of the net sensors, were dismissed at this step of the analysis. Subsequently, data were arithmetically transformed to the average reference, which was used for all analyses. Following artifact correction, ~70% of the 60 trials were retained. No significant differences in the number of retained trials or channels were observed when comparing the three affective contents.

Extraction of ssVEPs

Single epochs of 12,000 ms were averaged for each picture category separately, resulting in a time series containing significant amounts of stimulus-locked spectral power in the 10-Hz band. To further increase the sensitivity of the analysis to the 10-Hz oscillations that were evoked by the stimulus, a window procedure was applied to the averaged potential. A 500-ms Hanning window (containing five cycles of ssVEP) was shifted across the epoch in steps of 100 ms, and two types of analyses were conducted with the moving windows.

First, each window segment was transformed into the frequency domain using Discrete Fourier Transform (DFT) on 125 data points. The presence of significant power of evoked 10 Hz ssVEP signal was tested by means of the circular T-square statistic [Victor and Mast, 1991] applied to the Fourier coefficients of each window segment, at a sensor located at the occipital pole. The circular T-square algorithm is based on the ratio of circular variances calculated for the residuals with respect to a population mean and the empirical average. When setting the population mean to zero, this is a test for presence of a time-locked signal at the frequency of interest [here, 10 Hz using an *F*-distributed test statistic; Mast and Victor, 1991].

Second, window segments were successively averaged in the time domain, resulting in a representative time series of the ssVEP estimates with a high signal-to-noise ratio. From this time series, the cross-spectral density (CSD) matrix was computed for all sensor pairs and used in the beamformer estimation of the sources underlying the ssVEP. Both analyses were repeated for the baseline segment, which was used as a comparison to ensure that differences found in the ssVEP epoch were specific to the visual brain being driven by an external stimulus, and not to averaging spontaneous oscillatory activity.

Forward Model and Beamformer Source Estimation

A beamforming approach was chosen, combined with spatial coherence analysis as described by Gross et al. [2001], and implemented in the fieldtrip open source Matlab toolbox (http://www.ru.nl/fcdonders/fieldtrip). In this procedure, a spatial filter (beamformer) is calculated for each point p on a seeded grid in a realistic brain, based on the cross-spectral density matrix and the lead field of this source location. The beamformer is designed to capture the specific contribution of the source location p to the measured electric field, and suppress contributions from other source locations. The estimated power at p can be obtained by passing the multichannel EEG data through the spatial filter. Individually repeating the above procedure for each location on a three-dimensional grid in the brain results in a tomographic map of brain activity [Hillebrand and Barnes, 2005].

In the current study, a volume conduction model and leadfield (i.e., the solution of the forward model for specific orthogonal dipoles at the source locations described below) was calculated from individual Talairach-transformed MR images, which were segmented into scalp, skull, and brain compartments using the segmentation algorithm implemented in SPM 5 (http://www.fil.ion.ucl.ac.uk/spm/doc/). This resulted in an anatomically realistic three-shell model for each participant [Gross et al., 2001]. Source locations were seeded regularly at 4-mm distance of each other inside the brain compartment, and the leadfield was calculated as the solution of the forward model for three orthogonal dipoles at each of the grid locations source locations. The source space was restricted to the gray matter. Using this pre-defined space, the source activity at each grid point (i.e., each source location with three orthogonal model dipoles), in the dominant direction was estimated for the 10-Hz Fourier components extracted from the averaged ssVEP time series, using the beamformer spatial filters [see Gross et al., 2001, Appendix, for a detailed description of the procedure]. Regularization was applied to the cross-spectral density (CSD) matrix during inversion, as recommended by Gross et al. [2001]. A regularization parameter of 0.005*lambda1 (where lambda1 is the largest singular value of the CSD) was found to provide the best trade-off between spatial resolution and sensitivity to noise. The baseline segment and post-stimulus segment of each epoch were submitted to the beamformer algorithm separately, resulting in tomographical 10-Hz power representations for the baseline and viewing period in each condition, respectively.

In addition to power at each grid point, the spectral coherence across grid points was calculated [Gross et al., 2001]. Coherence between two time series is defined as the squared modulus of the time series' cross spectrum divided by the product of the power spectra of the time series. It thus represents correlation in the frequency domain and reaches high values (maximum of 1) when two time series have a constant phase difference, and 0 if they are uncoupled (i.e., temporally independent). Because the focus of this study was sensory-extrasensory coupling, we computed the spectral coherence between two reference locations at the bilateral occipital poles of each subject and every other grid location in the source volume. This procedure results in tomographical representations of coherence in which only areas are highlighted that are functionally related (i.e., showing high coherency) with each occipital pole.

Within each participant and condition, these two coherence maps were averaged to result in a single coherence map highlighting coupling between visual cortex and the other areas. Coherence between a reference area and itself is by definition 1 and was set to 0 manually to avoid distortion of the scale when plotting coherence maps. This measure does not indicate that there is high coherency across trials at the location itself, but that the phase is stable across the locations compared. The rationale for selecting reference locations in lower-tier visual cortex to study inter-site coherency over a period of 6,000 ms was as follows: on the basis of previous work, we assumed that the ssVEP should primarily drive early visual cortex. The reference points at the occipital poles thus helped us to (a) measure sensory-extrasensory coherency based on signals having high signal-to-noise ratios and (b) test our hypothesis of temporally sustained coupling between visual cortex and higher-order cortices at a fixed temporal rate, i.e., 10 Hz. This also implies that regions that exhibit coupling with the visual reference areas at a rate slower (or faster) than 10/s will not be visible in this analysis.

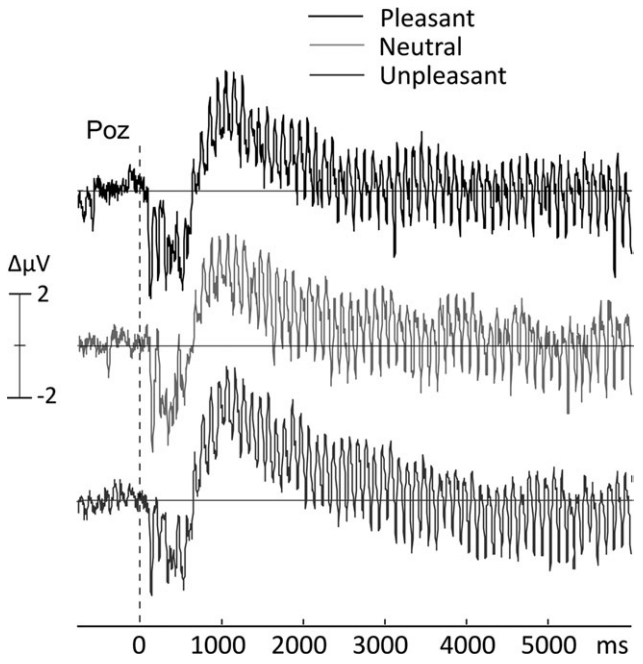

Figure 1.

Grand mean ($n = 11$) ssVEP time series at electrode site Poz, located just superior to the occipital pole. The three panels show the time domain averages over the entire viewing period (6,000 ms) for pleasant (top), neutral (middle), and unpleasant (bottom) pictures.

Statistical Parametric Mapping

The spectral power associated with picture viewing was compared to 10-Hz power at baseline for each grid location and participant by dividing the total power (baseline + ssVEP) by the ssVEP power, resulting in a normalized measure of change in power associate with picture viewing, bounded between 0 and 1. Coherence was likewise expressed as change from baseline. In this representation of the data, doubling of the power/coherence over baseline (corresponding to the 3 dB point) results in a value of 0.67, and values below 0.5 indicate a reduction below the baseline level.

For group analysis, each individual source space was transformed to an average brain obtained for the 11 participants using a linear transformation implemented in the fieldtrip toolbox. To evaluate effects of picture content on ssVEP amplitude across participants, paired *t* tests were performed on normalized power change and coherence at each grid point, comparing the three content conditions in a pair-wise fashion (pleasant vs. neutral, unpleasant vs. neutral, pleasant vs. unpleasant). Significance thresholds were determined by calculating a permutation distribution of *t* values for shuffled data to avoid alpha error accumulation [for a similar procedure see Keil et al., 2005]. In brief, 5,000 *t*-maps for each of the comparisons between the three contents (i.e., pleasant vs. neutral, unpleasant vs. neutral, pleasant vs. unpleasant) were calculated from data in which the conditions were randomly shuffled within each participant, and the maximum values of each map entered the permutation distribution. The 2.5 and 97.5% tails of the resulting distribution were then used to establish thresholds for *t* values indicating significant differences between picture contents. A mass univariate *t*-mapping approach was chosen here over factorial or multivariate designs, because this allows easier comparison with previous work on ssVEPs elicited by IAPS pictures [Keil et al., 2005], and the direction of any significant differences is more immediately evident, compared to an *F*-test.

For plotting purposes, the statistical maps were aligned with standard brain surfaces representing the cortical surface based on the MNI template brain transformed to fit native Talairach space and viewed using the AFNI surface mapper, SUMA [Saad et al., 2004]. Cortical structures with significant effects are reported in MNI coordinates. Because we did not observe differences between unpleasant and pleasant picture content (see results), *t*-maps that compared emotionally arousing (i.e., pleasant and unpleasant) and neutral content are illustrated.

TABLE I. Regions With Significant Changes in ssVEP Power

Cortical region	Hemisphere	Focus point MNI brain coordinates *x*	*y*	*z*	Statistic Relative change
Picture versus baseline					
Calcarine gyrus	L	−10	−86	−1	0.80
	R	11	−85	−9	0.92
Cuneus	L	−19	−78	7	0.82
	R	21	−80	5	0.91
Lingual gryrus	L	−22	−82	−5	0.69
	R	32	−75	−11	0.88
Middle occipital gyrus	L	−36	−71	5	0.70
	R	38	−66	7	0.79
Precuneus	L	−21	−45	48	0.70
Inferior temporal gyrus	R	54	−53	−21	0.67
Inferior parietal lobule	L	−48	−38	27	0.68
	R	54	−53	−21	0.67
Paracentral lobule	L	−14	−39	53	0.72
	R	6	−34	52	0.69
Precentral gyrus	R	33	−21	54	0.71
Postcentral gyrus	R	33	−35	45	0.72
		x	*y*	*z*	*t* value
Emotion versus neutral content					
Calcarine gyrus	L	−10	−86	−1	4.7
	R	11	−85	−9	3.9
Cuneus	L	−19	−78	7	4.3
	R	21	−80	5	5.6
Lingual gryrus	L	−22	−82	−5	3.7
	R	32	−75	−11	4.6
Middle occipital gyrus	L	−36	−71	5	4.3
	R	38	−66	7	4.6
Inferior temporal gyrus	L				
	R	54	−53	−21	3.7
Inferior parietal lobule	L	−48	−38	27	
	R	48	−33	30	

Note: Focus points within each region are given in MNI coordinates.

RESULTS

Figure 1 shows the grand mean ssVEP time series at electrode site Poz, located just superior to the occipital pole. The evoked oscillation at 10/s is clearly visible in the time domain, even prior to the moving window procedure described in the methods. Accordingly, spectral analysis showed a pronounced peak at 10 Hz in all participants and conditions, suggesting that the ssVEP procedure was effective. This was confirmed by the circular T-square analysis performed at the occipital pole sensor, which resulted in *F*-values exceeding 8.2 (all P values < 0.001) in each participant and condition. Normalized change in ssVEP power over baseline is shown in Figure 2, for pleasant, neutral, and unpleasant picture contents. Brain areas in which the stimulus-locked ssVEP power accounted for at least 67% of the total power in the entire recording epoch (baseline plus ssVEP) included the ventral and lateral occipital cortex, bilateral portions of the medial and inferior temporal gyrus, the bilateral precuneus, inferior parietal lobule, and postcentral gyrus (see Table I, upper panel).

Permutation-controlled Student's *t* tests between the three contents were then performed for all voxels. When comparing pleasant and unpleasant contents, these tests did not exceed the critical *t* value of 3.6, which corresponded to the permutation-controlled alpha level of 0.05. Replicating previous data [Moratti et al., 2004], ssVEPs were most sensitive to the distinction between emotionally arousing (pleasant or unpleasant) and non-emotional or neutral pictures. Therefore, data from the pleasant and unpleasant conditions were averaged to form one condition representing emotionally arousing content. Figure 3 illustrates the contrast in power when viewing emotional

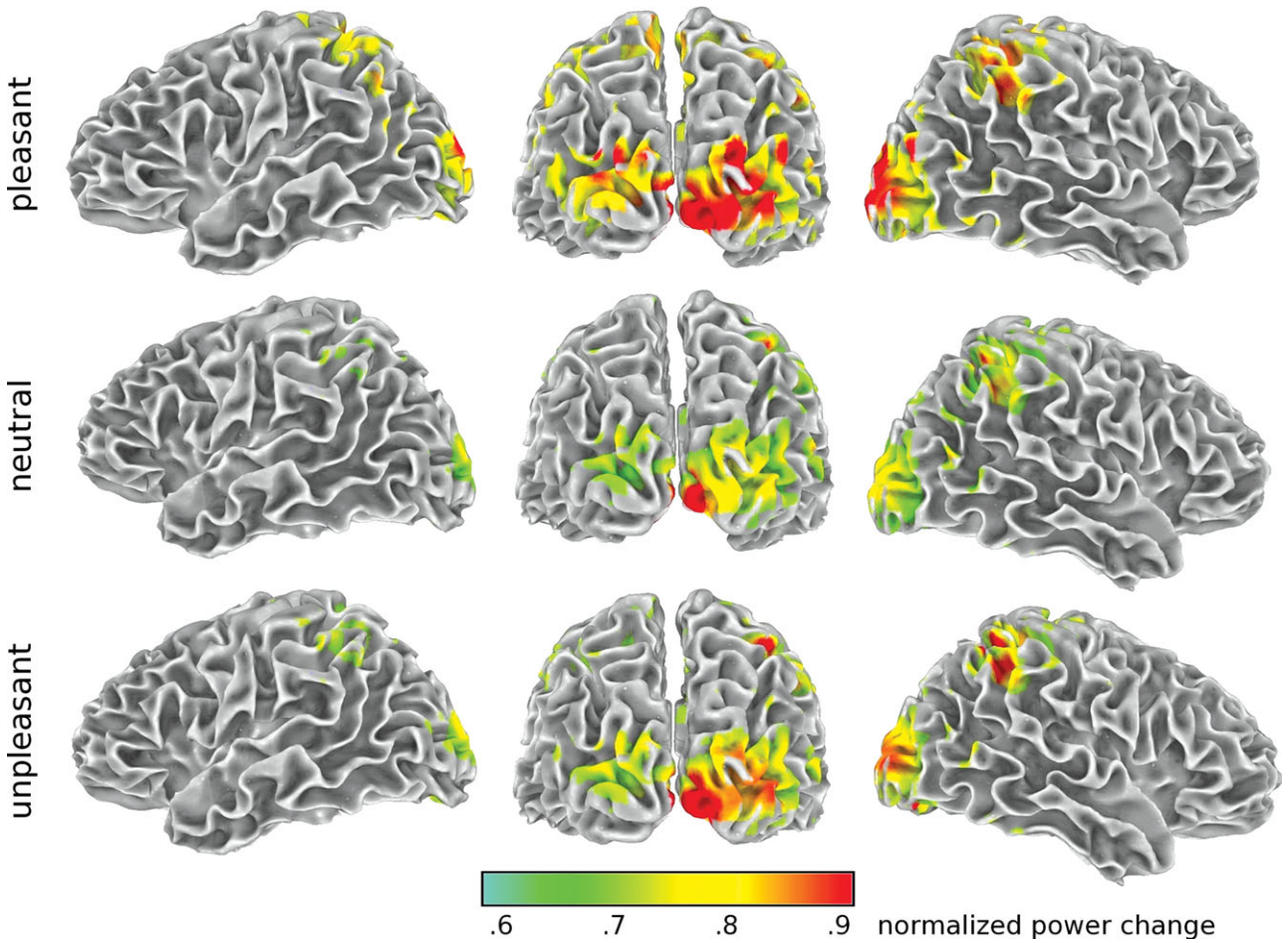

Figure 2.

Normalized power change at the ssVEP frequency when viewing flickering pictures, compared to a prestimulus baseline. Areas with at least twice the power of the baseline are highlighted for pleasant, neutral, and unpleasant pictures. Note that the spatial accuracy of the source projection is limited by factors inherent in the projection method (e.g., selection of grid points) and the interpolation of individual results to a standard brain for group analysis. A standard brain surface (gray/white matter border) is shown with red colors indicating greater change of power at the ssVEP frequency, compared to baseline.

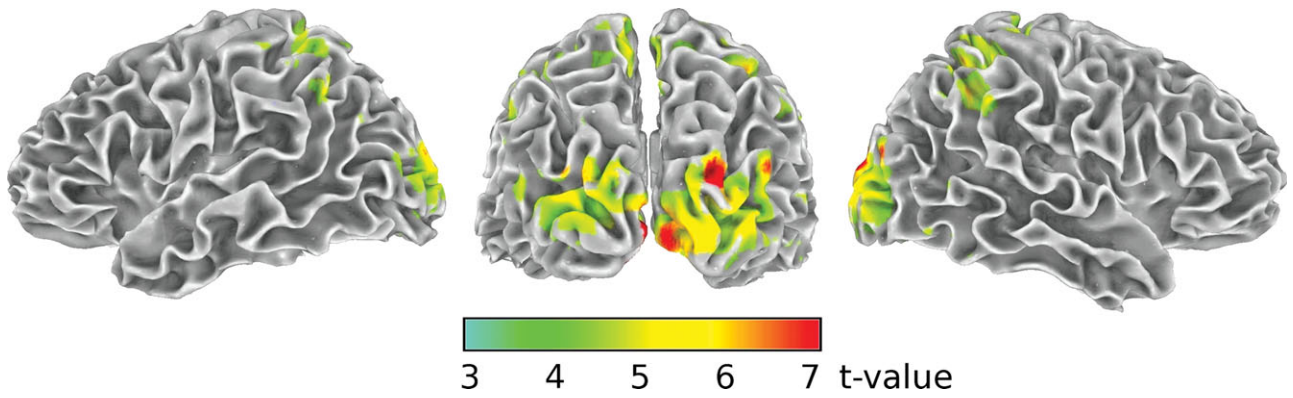

Figure 3.

Maps of permutation controlled *t* tests comparing ssVEP power when viewing emotionally arousing (pleasant and unpleasant) and neutral pictures. Regions are highlighted that show above threshold difference in 10-Hz spectral power when viewing emotionally arousing, compared to neutral, pictures.

(pleasant and unpleasant) pictures, compared to viewing neutral pictures, thresholded at the critical t value of 3.6 ($P < 0.05$ corrected). Stimulus-locked ssVEP power was enhanced for emotionally arousing pictures in lateral occipital cortices and in the same parietal areas—bilateral precuneus and intraparietal lobules—where spectral power was generally enhanced following picture onset (see Table I, lower panel).

Similar to effects for spectral power, spectral coherence between the bilateral occipital poles and the rest of the brain was expressed as change over baseline. This resulted in maps highlighting areas with significant coherence change during the ssVEP period, compared to baseline (see Fig. 4). Doubling of spectral coherence over baseline in the 10-Hz band was observed in widespread cortical areas of the left hemisphere, including the cuneus and precuneus, superior and inferior temporal gyrus, inferior frontal cortex, and insula (see Table II, upper panel). For the right hemisphere, coherence changes were observed in the precuneus, superior temporal gyrus, angular gyrus, inferior frontal, and perimotor cortex.

In a subsequent step, change in spectral coherence was compared across picture contents. Permutation-controlled Student's t tests determined a critical t value of 3.4 (corresponding to a two-tailed, 0.05 corrected alpha level) and again the comparison of pleasant and unpleasant content showed no differences. Thus, data from the pleasant and unpleasant conditions were averaged and compared to neutral picture viewing. Figure 5 displays the t-map comparing normalized coherence relative to the occipital poles when viewing emotional compared to neutral pictures. When viewing emotionally arousing pictures a significant increase in coupling with the occipital cortex was observed in the left medial and inferior temporal gyrus, bilateral precuneus and intraparietal lobules, and the right middle frontal gyrus. A complete list of regions is found in Table II, lower panel.

TABLE II. Regions With Significant Changes in ssVEP Coherence Relative to the Bilateral Occipital Poles

Cortical region	Hemisphere	Focus point MNI brain coordinates x	y	z	Statistic Normalized coherence change
Picture versus baseline					
Middle occipital gyrus	L	−29	−77	−3	0.74
Precuneus	L	−18	−63	35	0.88
	R	14	−62	38	0.73
Inferior/superior parietal lobule	L	−27	−53	41	0.89
Angular/supramarginal gyrus	L	−39	−58	−26	0.71
Insula	L	−32	16	−10	0.72
Middle temporal gyrus	L	−56	−37	1	0.74
Superior temporal gyrus	R	59	−17	9	0.73
Inferior temporal gyrus	L	−58	−7	−27	0.72
	R				
Temporal pole	L	−53	27	−25	0.80
	R	39	25	−28	0.72
Postcentral gyrus	L	−53	−24	35	0.78
	R	47	−29	41	0.80
Precentral gyrus	R	60	4	24	0.72
Inferior/middle frontal gyrus	R	41	44	5	0.68
Inferior frontal gyrus	L	−47	44	−12	0.79
		x	y	z	t value
Emotion versus neutral content					
Precuneus	R	16	−53	48	6.2
Inferior/superior parietal lobule	L	−33	−45	39	4.7
	R	28	−36	47	3.4
Middle/inferior temporal gyrus	L	−58	−17	−24	4.4
Postcentral gyrus	L	−41	−37	44	4.3
Paracentral lobule	L	−14	−39	53	4.2
	R	6	−34	52	4.1
Inferior/middle frontal gyrus	R	40	60	−6	3.7

Focus points within each region are given in MNI coordinates.

DISCUSSION

This study used frequency tagging as a means to determine cortical structures that are coactive with the visual cortex during processing of emotional pictures. To this end, we capitalized on the spatial information inherent in individual structural brain anatomy. Source projections were based on individual realistic head models and coherence analysis was employed to identify cortical regions showing temporal coupling. Participants viewed perceptually balanced pleasant, neutral, and unpleasant pictures, flickering at 10 Hz, which resulted in a strong ssVEP signal, maintained for 6,000 ms (i.e., as long as the flickering pictures were present). This signal was averaged across trials and within trials [Keil et al., 2008], to establish a reliable estimate of evoked (i.e., stimulus-locked) power in the 10-Hz band. The data replicated previous research, which was limited to scalp data or source estimations with less spatial resolution [Keil et al., 2003; Kemp et al., 2002; Moratti et al., 2004], in that heightened ssVEP power was obtained when participants viewed emotionally arousing, compared to neutral, pictures.

Using each participant's individual anatomical information to improve the spatial sensitivity of our analysis, cortical regions were identified that showed significant enhancement of evoked ssVEP when participants viewed flickering pictures, compared to a pre-stimulus baseline. These regions extended well beyond occipital visual cortex. Massive averaging—across and within trials—that we applied to the data amplified the portion of the spectrum that was strictly phase-locked to the external 10-Hz flicker. Therefore, the finding of significant ssVEP power

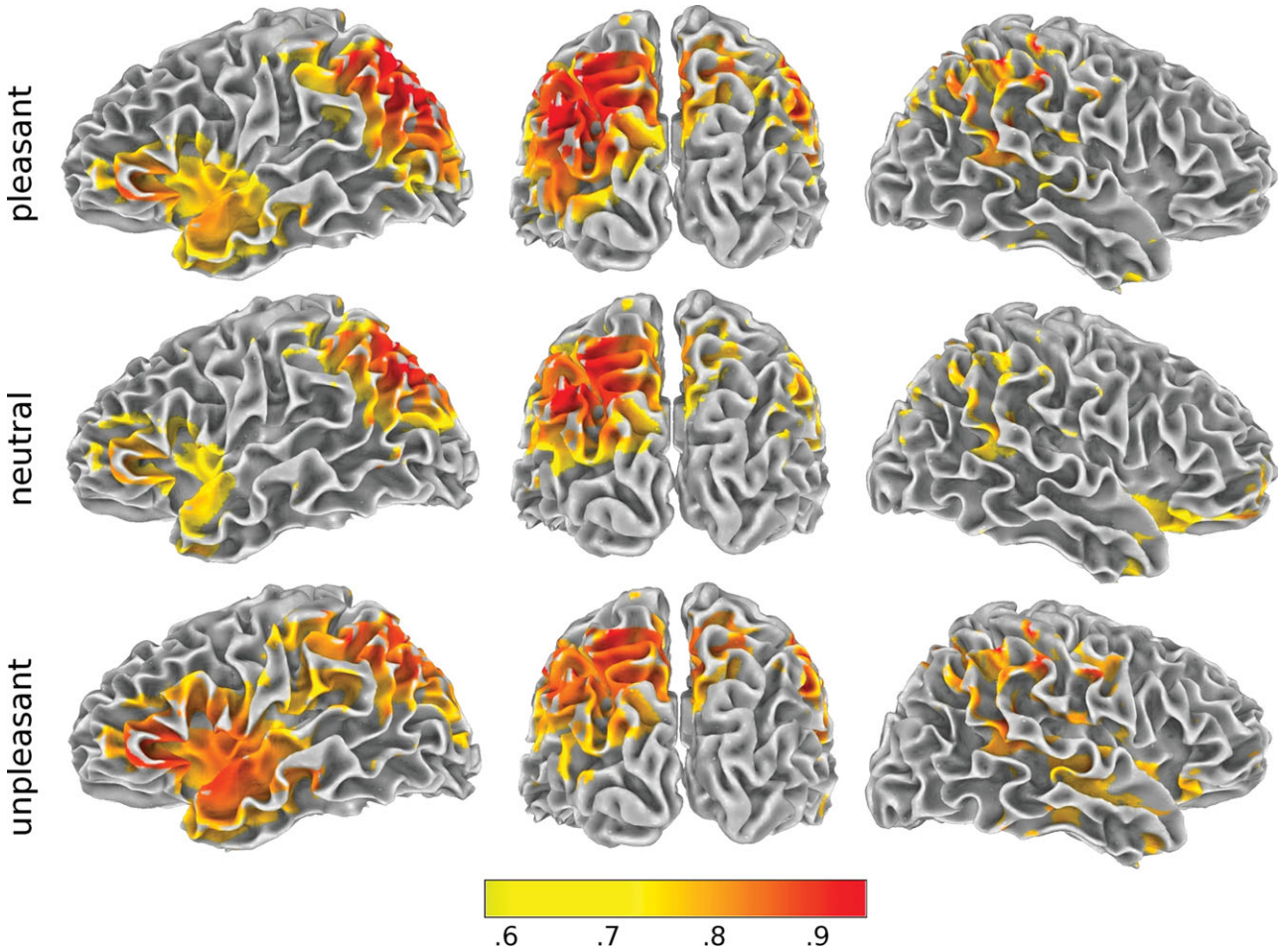

Figure 4.

Normalized inter-site coherence change at the ssVEP frequency when viewing flickering pictures, compared to a prestimulus baseline. Coherence was measured between reference locations at the bilateral medial occipital poles (providing the reference signal), where the ssVEP signal was most pronounced, and the remainder of the cortical gray matter (providing the comparison signals). Areas with at least a doubling of prestimulus inter-site coherence are highlighted for pleasant, neutral, and unpleasant pictures, showing reliable and similar changes in coherence when viewing the flickering stimuli. This measure does not indicate that there is high coherency across trials at the location itself, but that the phase is stable across the locations compared.

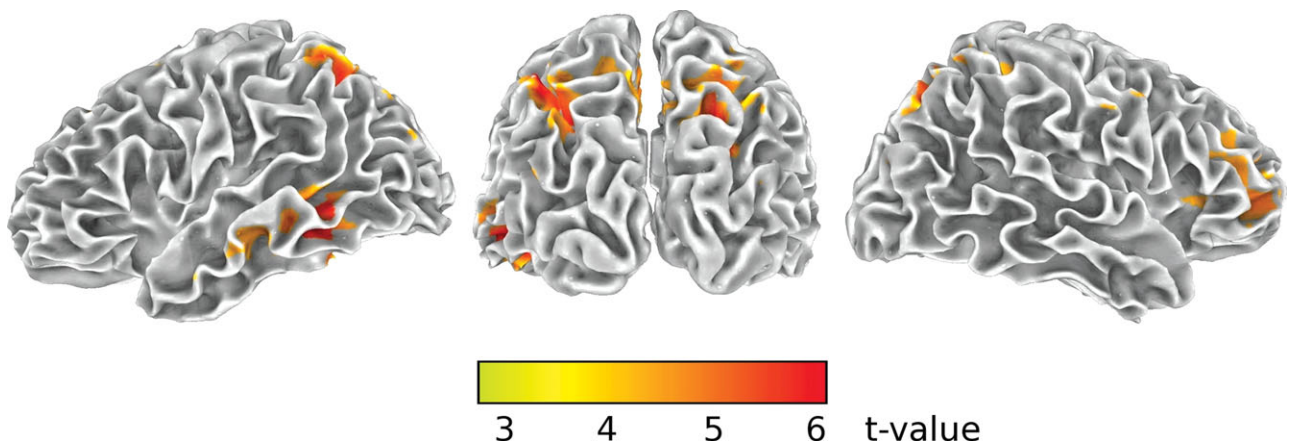

Figure 5.

Maps of permutation controlled *t* tests on inter-site coherence values comparing emotionally arousing (pleasant and unpleasant) to neutral pictures. Regions are highlighted that show greater coupling with bilateral visual cortex when viewing emotionally arousing, compared to neutral, pictures.

modulation in inferior temporal and dorsal parietal visual cortex suggests that the flicker systematically and rhythmically engaged visual association cortex, resonating with the brightness-modulated stimulus train at a frequency of 10 Hz. This suggests a close functional relationship between early visual and temporo-parietal areas during rapid serial visual processing. The present data imply that these functional links operate at a steady repetitive rate, suggesting rapid connections between visual and extra-visual areas. In terms of laterality, earlier work reported that the left hemisphere shows a preponderance of ssVEP power during stimulation with complex IAPS pictures, whereas phase synchrony is often more pronounced on the right [Keil et al., 2005].

The fact that many visual associative structures showed resonance with the 10-Hz flicker and coherent temporal relationships with occipital visual cortex is consistent with hypotheses that visual representations formed during ssVEP stimulation are not established independently and *de novo* for each cycle, but that information from previous cycles is retained in a functionally coupled neural network including sensory as well as higher-order areas [Härle et al., 2004; Keil et al., 2007]. In the present study, oscillatory network communication was established as a distributed set of connected regions coherently engaged and disengaged in synchrony with the reference location in the visual cortex, at a rate of 10 oscillations s^{-1}. Coordinated activity in such functional networks may assist in the formation of predictions regarding the nature of incoming stimuli in a given context [Engel et al., 2001]. Although it is possible that widespread coordinated activity is specific to complex stimuli such as IAPS pictures and is not seen with more simple stimuli (faces, geometric shapes) often used in the cognitive neuroscience laboratory, photographs as used here are most similar to the visual scenes processed in daily life. In the laboratory, on the other hand, simplistic grating stimuli receiving motivational relevance through classical conditioning have been shown to be associated with more circumscribed connectivity that is constrained to the occipital lobe [Keil et al., 2007]. This suggests that more ecologically valid, complex visual scenes engage a broader array of cortical structures in a coherent fashion, which probably reflects an integrative neural mechanism linking complex visual information to semantic content and behavioral response representations that are important for relevant action.

To further examine the spatio-temporal structure of such tightly coupled cortical networks, inter-area coupling was quantified by means of coherence analysis [Nunez et al., 1997]. It is crucial for spatio-temporal analysis of brain electric activity that false positives due to volume conduction, choice of reference electrodes, etc., are avoided [Nunez et al., 1999]. In the current study, we adopted multiple strategies to reduce effects leading to spurious differences in coherence: first, the beamforming approach enhances spatially independent activity [Gross et al., 2001] by actively suppressing the contributions of other, temporally identical, sources to a given location in the source model (see Methods). Second, we examined differences between picture contents, thus keeping any residual, nonspecific, influences on the measurement of coherence constant. This approach highlights content-related changes of power and coherence that were under experimental control, as recommended by Nunez et al. [1999]. A further methodological improvement over earlier work concerns the constraints of source projections. Beamforming depends to a large extent on the validity of the volume conductor model and its relationship with the sensor space, i.e., the leadfield [Huang et al., 2004], and here we used realistic head models derived from individual anatomy as reflected in the high resolution structural MRI data.

In terms of large-scale neurophysiology, the oscillatory functional network observed in this study may provide reentrant feedback to visual areas, originating from higher order visual cortices, and following an initial bottom-up cascade of visual analysis in each cycle of processing [Martinez et al., 1999]. Work examining classical conditioning with simple visual stimuli has suggested that local connectivity within the extended visual cortex increases with prolonged exposure to the learning regime [Keil et al., 2007]. Thus, one could speculate that re-entrant modulation from anterior, distant structures is reduced over trials, giving rise to more effective, highly connected local networks in the occipital lobe [Gruber et al., 2004]. Work in experimental animals has demonstrated strong re-entrant connections into visual cortex originating in the amygdala [Amaral et al., 2003]. The present study supports that such feedback may also arise from higher-order (parietal and frontal) cortical areas and may act to enhance sensitivity of visual neurons coding for motivationally relevant features present in the field of view, as hypothesized in the context of spatial attention [Hamker, 2005] as well as classical and instrumental conditioning [Keil, 2004]. In this vein, the ssVEP as a measure of ongoing stimulus processing in visual cortex might be able to reflect biasing signals from higher-order cortical areas [Kastner and Ungerleider, 2000], changing the sensitivity of visual cortical neurons in favor of features associated with emotionally arousing content.

The present data provide evidence that (i) increased coupling for arousing content occurs for large-scale (neural mass) electrical activity on the cortical level, and (ii) the cortical regions tagged as elements in such a functional network are consistent with regions identified by means of functional imaging. Taken together, this suggests that cortical structures interact in a rapid fashion, establishing networks linking perceptual features to attentive behavior and ultimately action preparation.

REFERENCES

Aftanas LI, Reva NV, Varlamov AA, Pavlov SV, Makhnev VP (2004): Analysis of evoked EEG synchronization and desynchronization in conditions of emotional activation in humans: Temporal and topographic characteristics. Neurosci Behav Physiol 34:859–867.

Amaral DG, Behniea H, Kelly JL (2003): Topographic organization of projections from the amygdala to the visual cortex in the macaque monkey. Neuroscience 118:1099–1120.

Bradley MM, Sabatinelli D, Lang PJ, Fitzsimmons JR, King W, Desai P (2003): Activation of the visual cortex in motivated attention. Behav Neurosci 117:369–380.

Costa VD, Lang PJ, Sabatinelli D, Versace F, Bradley MM (2010): Emotional imagery: Assessing pleasure and arousal in the brain's reward circuitry. Hum Brain Mapp 31:1446–1457.

Desimone R (1996): Neural mechanisms for visual memory and their role in attention. Proc Natl Acad Sci USA 93:13494–13499.

Di Russo F, Pitzalis S, Aprile T, Spitoni G, Patria F, Stella A, Spinelli D, Hillyard SA (2007): Spatiotemporal analysis of the cortical sources of the steady-state visual evoked potential. Hum Brain Mapp 28:323–334.

Engel AK, Fries P, Singer W (2001): Dynamic predictions: Oscillations and synchrony in top-down processing. Nat Rev Neurosci 2:704–716.

Gross J, Kujala J, Hamalainen M, Timmermann L, Schnitzler A, Salmelin R (2001): Dynamic imaging of coherent sources: Studying neural interactions in the human brain. Proc Natl Acad Sci USA 98:694–699.

Gruber T, Malinowski P, Muller MM (2004): Modulation of oscillatory brain activity and evoked potentials in a repetition priming task in the human EEG. Eur J Neurosci 19:1073–1082.

Hamker FH (2005): The reentry hypothesis: The putative interaction of the frontal eye field, ventrolateral prefrontal cortex, and areas V4, IT for attention and eye movement. Cereb Cortex 15:431–447.

Härle M, Rockstroh BS, Keil A, Wienbruch C, Elbert TR (2004): Mapping the brain's orchestration during speech comprehension: Task-specific facilitation of regional synchrony in neural networks. BMC Neurosci 5:40.

Herrmann CS (2001): Human EEG responses to 1–100 Hz flicker: Resonance phenomena in visual cortex and their potential correlation to cognitive phenomena. Exp Brain Res 137:346–353.

Hillebrand A, Barnes GR (2005): Beamformer analysis of MEG data. Int Rev Neurobiol 68:149–171.

Huang MX, Shih JJ, Lee RR, Harrington DL, Thoma RJ, Weisend MP, Hanlon F, Paulson KM, Li T, Martin K, Millers GA, Canive JM (2004): Commonalities and differences among vectorized beamformers in electromagnetic source imaging. Brain Topogr 16:139–158.

Junghöfer M, Elbert T, Leiderer P, Berg P, Rockstroh B (1997): Mapping EEG-potentials on the surface of the brain: A strategy for uncovering cortical sources. Brain Topogr 9:203–217.

Junghofer M, Elbert T, Tucker DM, Rockstroh B (2000): Statistical control of artifacts in dense array EEG/MEG studies. Psychophysiology 37:523–532.

Kastner S, Ungerleider LG (2000): Mechanisms of visual attention in the human cortex. Annu Rev Neurosci 23:315–341.

Keil A (2004): The role of human prefrontal cortex in motivated perception and behavior: A macroscopic perspective. In: Otani S, editor. Prefrontal Cortex: From Synaptic Plasticity to Cognition. New York: Kluwer. pp 245–267.

Keil A, Gruber T, Muller MM, Moratti S, Stolarova M, Bradley MM, Lang PJ (2003): Early modulation of visual perception by emotional arousal: Evidence from steady-state visual evoked brain potentials. Cogn Affect Behav Neurosci 3:195–206.

Keil A, Moratti S, Sabatinelli D, Bradley MM, Lang PJ (2005): Additive effects of emotional content and spatial selective attention on electrocortical facilitation. Cereb Cortex 15:1187–1197.

Keil A, Stolarova M, Moratti S, Ray WJ (2007): Adaptation in visual cortex as a mechanism for rapid discrimination of aversive stimuli. Neuroimage 36:472–479.

Keil A, Smith JC, Wangelin B, Sabatinelli D, Bradley MM, Lang PJ (2008): Electrocortical and electrodermal responses co-vary as a function of emotional arousal: A single-trial analysis. Psychophysiology 45:511–515.

Keil A, Sabatinelli D, Ding M, Lang PJ, Ihssen N, Heim S (2009): Re-entrant projections modulate visual cortex in affective perception: Directional evidence from granger causality analysis. Hum Brain Mapp 30:532–540.

Kemp AH, Gray MA, Eide P, Silberstein RB, Nathan PJ (2002): Steady-state visually evoked potential topography during processing of emotional valence in healthy subjects. Neuroimage 17:1684–1692.

Lachaux JP, Chavez M, Lutz A (2003): A simple measure of correlation across time, frequency and space between continuous brain signals. J Neurosci Methods 123:175–188.

Lang PJ (1980): Behavioral treatment and bio-behavioral assessment: Computer applications. In: Sidowski JB, Johnson JH, William TA, editors. Technology in Mental Health Care Delivery Systems. Norwood, NJ: Ablex. pp 119–137.

Lang PJ, Bradley MM (2010): Emotion and the motivational brain. Biol Psychol 83:437–450.

Lang PJ, Bradley MM, Fitzsimmons JR, Cuthbert BN, Scott JD, Moulder B, Nangia V (1998): Emotional arousal and activation of the visual cortex: An fMRI analysis. Psychophysiology 35:199–210.

Lang PJ, Bradley MM, Cuthbert BN (2005): International Affective Picture System: Technical Manual and Affective Ratings. Gainesville, FL: NIMH Center for the Study of Emotion and Attention.

Martinez A, Anllo-Vento L, Sereno MI, Frank LR, Buxton RB, Dubowitz DJ, Wong EC, Hinrichs H, Heinze HJ, Hillyard SA (1999): Involvement of striate and extrastriate visual cortical areas in spatial attention. Nat Neurosci 2:364–369.

Mast J, Victor JD (1991): Fluctuations of steady-state VEPs: Interaction of driven evoked potentials and the EEG. Electroencephalogr Clin Neurophysiol 78:389–401.

McMains SA, Fehd HM, Emmanouil TA, Kastner S (2007): Mechanisms of feature- and space-based attention: Response modulation and baseline increases. J Neurophysiol 98:2110–2121.

Michel CM, Murray MM, Lantz G, Gonzalez S, Spinelli L, Grave de Peralta R (2004): EEG source imaging. Clin Neurophysiol 115:2195–2222.

Moratti S, Keil A (2005): Cortical activation during Pavlovian fear conditioning depends on heart rate response patterns: An MEG study. Brain Res Cogn Brain Res 25:459–471.

Moratti S, Keil A (2009): Not what you expect: Experience but not expectancy predicts conditioned responses in human visual and supplementary cortex. Cereb Cortex 19:2803–2809.

Moratti S, Keil A, Stolarova M (2004): Motivated attention in emotional picture processing is reflected by activity modulation in cortical attention networks. Neuroimage 21:954–964.

Müller MM, Malinowski P, Gruber T, Hillyard SA (2003): Sustained division of the attentional spotlight. Nature 424:309–312.

Nunez PL, Srinivasan R, Westdorp AF, Wijesinghe RS, Tucker DM, Silberstein RB, Cadusch PJ (1997): EEG coherency. I: Statistics, reference electrode, volume conduction, Laplacians, cortical imaging, and interpretation at multiple scales. Electroencephalogr Clin Neurophysiol 103:499–515.

Nunez PL, Silberstein RB, Shi Z, Carpenter MR, Srinivasan R, Tucker DM, Doran SM, Cadusch PJ, Wijesinghe RS (1999): EEG coherency II: Experimental comparisons of multiple measures. Clin Neurophysiol 110:469–486.

Regan D (1989): Human Brain Electrophysiology: Evoked Potentials and Evoked Magnetic Fields in Science and Medicine. New York: Elsevier.

Saad ZS, Reynolds RC, Argall BD, Japee S, Cox RW (2004): SUMA:an interface for surface-based intra- and inter-subject analysis with AFNI. In: Proceedings of the 2004 IEEE International Symposium on Biomedical Imaging, Arlington, VA. New York: IEEE .p 1510–1513.

Sabatinelli D, Bradley MM, Fitzsimmons JR, Lang PJ (2005): Parallel amygdala and inferotemporal activation reflect emotional intensity and fear relevance. Neuroimage 24:1265–1270.

Sabatinelli D, Lang PJ, Keil A, Bradley MM (2007): Emotional perception: Correlation of functional MRI and event related potentials. Cereb Cortex 17:1066–1073.

Sabatinelli D, Lang PJ, Bradley MM, Costa VD, Keil A (2009): The timing of emotional discrimination in human amygdala and ventral visual cortex. J Neurosci 29:14864–14868.

Silberstein RB, Ciorciari J, Pipingas A (1995): Steady-state visually evoked potential topography during the Wisconsin card sorting test. Electroencephalogr Clin Neurophysiol 96:24–35.

Victor JD, Mast J (1991): A new statistic for steady-state evoked potentials. Electroencephalogr Clin Neurophysiol 78: 378–388.

Vuilleumier P, Driver J (2007): Modulation of visual processing by attention and emotion: Windows on causal interactions between human brain regions. Philos Trans R Soc Lond B Biol Sci 362:837–855.

Ward DM, Jones RD, Bones PJ, Carroll GJ (1999): Enhancement of deep epileptiform activity in the EEG via 3-D adaptive spatial filtering. IEEE Trans Biomed Eng 46:707–716.

Yantis S (2008): The neural basis of selective attention: Cortical sources and targets of attentional modulation. Curr Dir Psychol Sci 17:86–90.

APPENDIX

IAPS Numbers Used in This Study

1019	1026	1050	1052	1090	1110	1111	1113	1114	1120	1440	1441
1460	1463	1540	1590	1610	1710	1750	1920	2191	2214	2215	2372
2383	2393	2394	2480	2595	3000	3051	3060	3068	3069	3071	3100
3101	3266	3400	4611	4658	4659	4666	4676	4677	4680	4681	4690
4694	5740	7036	7041	7050	7100	7130	7161	7224	7234	7500	7550